

Design of highly potent urea-based, exosite-binding inhibitors selective for glutamate carboxypeptidase II

Jan Tykvart, Jiri Schimer, Andrej Jancarik, Jitka Barinkova, Vaclav Navratil, Jana Starkova, Karolina Sramkova, Jan Konvalinka, Pavel Majer, and Pavel Sacha

J. Med. Chem., **Just Accepted Manuscript** • DOI: 10.1021/acs.jmedchem.5b00278 • Publication Date (Web): 29 Apr 2015

Downloaded from <http://pubs.acs.org> on May 6, 2015

Just Accepted

“Just Accepted” manuscripts have been peer-reviewed and accepted for publication. They are posted online prior to technical editing, formatting for publication and author proofing. The American Chemical Society provides “Just Accepted” as a free service to the research community to expedite the dissemination of scientific material as soon as possible after acceptance. “Just Accepted” manuscripts appear in full in PDF format accompanied by an HTML abstract. “Just Accepted” manuscripts have been fully peer reviewed, but should not be considered the official version of record. They are accessible to all readers and citable by the Digital Object Identifier (DOI®). “Just Accepted” is an optional service offered to authors. Therefore, the “Just Accepted” Web site may not include all articles that will be published in the journal. After a manuscript is technically edited and formatted, it will be removed from the “Just Accepted” Web site and published as an ASAP article. Note that technical editing may introduce minor changes to the manuscript text and/or graphics which could affect content, and all legal disclaimers and ethical guidelines that apply to the journal pertain. ACS cannot be held responsible for errors or consequences arising from the use of information contained in these “Just Accepted” manuscripts.



Design of highly potent urea-based, exosite-binding inhibitors selective for glutamate carboxypeptidase II

Jan Tykvart^{1,2‡}, Jiří Schimer^{1,2‡}, Andrej Jančařík¹, Jitka Bařínková¹, Václav Navrátil^{1,2}, Jana Starková¹, Karolína Šrámková¹, Jan Konvalinka^{1,2*}, Pavel Majer¹ and Pavel Šácha^{1,2*}

¹Gilead Sciences and IOCB Research Centre, Institute of Organic Chemistry and Biochemistry, Academy of Sciences of the Czech Republic, Flemingovo n. 2, Prague 6, Czech Republic

²Department of Biochemistry, Faculty of Science, Charles University, Albertov 6, Prague 2, Czech Republic

KEYWORDS: PSMA, GCPII, GCPIII, inhibitor selectivity, imaging, structure-aided drug design

ABSTRACT: We present here a structure-aided design of inhibitors targeting the active site as well as exosites of glutamate carboxypeptidase II (GCPII), a prostate cancer marker, preparing potent and selective inhibitors that are more than 1000-fold more active toward GCPII than its closest human homolog, glutamate carboxypeptidase III (GCPIII). Additionally, we demonstrate that the prepared inhibitor conjugate can be used for sensitive and selective imaging of GCPII in mammalian cells.

INTRODUCTION

Prostate carcinoma (PCa) was the most commonly diagnosed cancer and the leading cause of cancer death among men in the United States in 2014, with an estimated 233,000 diagnoses and 30,000 deaths.¹ Glutamate carboxypeptidase II (GCPII), also known as prostate specific membrane antigen (PSMA), is a promising biomarker of this pathological condition.²⁻⁵ Additionally, GCPII has been investigated as a potential biomarker of other solid tumors because of its reported expression in tumor neovasculature.⁶⁻⁷

Low-molecular-weight inhibitors can be used to target GCPII.^{2, 8-10} Specificity of these inhibitors is an issue that needs to be properly addressed, to exclude any possible off-target effects. In principle, any close homolog with similar enzymatic activity is likely to be affected by these targeting inhibitors. Glutamate carboxypeptidase III (GCPIII) is the most likely candidate for off-target activity of GCPII inhibitors. GCPIII shares 67% sequence identity with GCPII and has similar enzymatic activity.¹¹⁻¹² Its tissue distribution is similar to that of GCPII, according to RT-PCR analyses, but it is more highly expressed in the testes, ovaries, and placenta.¹²⁻¹³ In addition to its “GCPII-like activity,” GCPIII was recently also shown to degrade β -citrylglutamate (BCG).¹³ Even though the physiological function of this pseudopeptide remains unknown, it may play an important role in spermatogenesis and brain development, based on its elevated expression in testicular germinal cells and newborn brain tissue.¹⁴⁻¹⁵ Additionally, BCG has been proposed to serve as an iron chelator.¹⁶⁻¹⁷ Currently, GCPIII is the only known enzyme responsible for BCG degradation, and no data are available for educated assessment of the potential disruption of BCG metabolism by inhibition of GCPIII. To the best of our knowledge, no studies investigating GCPII-targeting inhibitors have yet analyzed their activity towards GCPIII. Analysis of the specificity of these inhibitors

is essential to facilitate their development as potential theranostic agents for PCa.

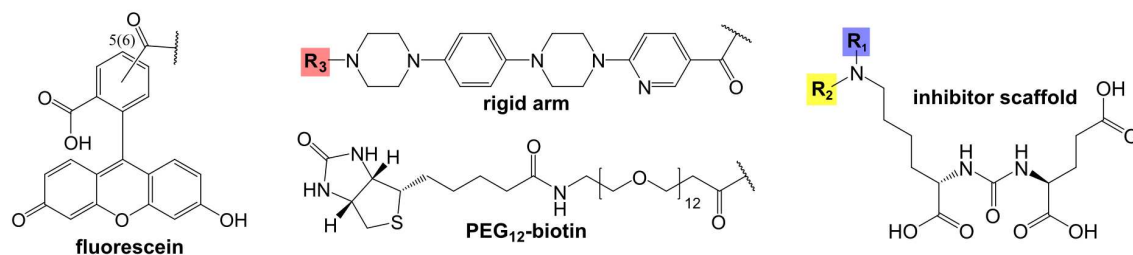
Recently, we reported the structure-activity relationship study of GCPII inhibitors modified with linkers and biotin molecules, which enable facile preparation of GCPII-targeting nanoparticles.¹⁸ Nevertheless, the GCPII inhibitors with PEG linkers showed slightly decreased inhibitory potency. In the present work, we set out to improve their potency by increasing the linker's rigidity. Additionally, we set out to investigate the specificity of these inhibitors against GCPIII.

RESULTS AND DISCUSSION

To decrease the mobility of the linker region, we designed a rigid arm formed by joined pyridine, piperazine, and benzene rings. As shown in Figure 1, the addition of this rigid arm led to a 15-fold increase in potency for inhibitors with terminal PEG₁₂-biotin [compare $K_i(\mathbf{3}) = 1.6$ nM to $K_i(\mathbf{6}) = 0.11$ nM] but did not affect the potency of inhibitors with terminal acetyl groups [compare $K_i(\mathbf{2}) = 45$ pM to $K_i(\mathbf{5}) = 49$ pM]. As we showed previously, inhibitor conjugates with a terminal PEG₁₂-biotin moiety can be used to easily modify nanoparticles *via* the biotin-streptavidin interaction.¹⁸ The improvement in inhibitor potency should also affect the binding properties of the nanoparticles.

Additionally, because the length of the rigid arm should be sufficient to reach outside the GCPII entrance funnel, we prepared a small-molecule agent for visualization of GCPII by replacing the terminal PEG₁₂-biotin with a fluorophore (compound **7**). Interestingly, the addition of fluorescein moiety resulted in a further improvement of inhibitor potency, leading to a picomolar inhibition constant [$K_i(\mathbf{7}) = 8.6$ pM].

To elucidate the binding mechanism of the inhibitors with the rigid arm, we prepared diffraction-quality crystals of



Cmp	R ₁	R ₂	R ₃	Avi-GCPII K _i [nM]	Avi-GCPIII K _i [nM]	selectivity
1	H	CH ₃	-	0.17 ± 0.03*	8.2 ± 1.1	48
2	Br	CH ₃	-	0.045 ± 0.005*	14 ± 2	310
3	Br	PEG ₁₂ -biotin	-	1.6 ± 0.1*	300 ± 10	190
4	H	rigid arm	CH ₃	0.071 ± 0.002	100 ± 10	1400
5	Br	rigid arm	CH ₃	0.049 ± 0.003	210 ± 10	4200
6	Br	rigid arm	PEG ₁₂ -biotin	0.11 ± 0.01	730 ± 10	6600
7	Br	rigid arm	fluorescein	0.0086 ± 0.0009	16 ± 1	1900

Figure 1. Structures and inhibition constants of GCPII inhibitors. The compounds were derived from a urea-based inhibitor scaffold. The ϵ -amino group of lysine was subsequently modified, and the IC₅₀ values for Avi-GCPII and Avi-GCPIII were determined using an HPLC-based enzymatic assay with folyl- γ -L-glutamate (FolGlu) as substrate. K_i values were subsequently calculated using Cheng-Prusoff equation for competitive inhibition mode and kinetic parameters of substrate cleavage in reaction buffer ($K_M(\text{Avi-GCPII}) = 38.6 \pm 2.3 \text{ nM}$ ¹⁸ and $K_M(\text{Avi-GCPIII}) = 1020 \pm 40 \text{ nM}$) and are shown as means with standard error (SE) from duplicate experiments. The selectivity represents the fold difference in K_i values for Avi-GCPII and Avi-GCPIII. *K_i values taken from ref.¹⁸

Avi-GCPII in complex with **7**. We solved the structure by molecular replacement and refined the final model to 1.86 Å resolution (PDB code 4X3R; data collection and refinement statistics are shown in the Supporting Information). We identified a clear electron density map for the portion of **7** comprising the inhibitor scaffold, bromobenzyl moiety, and first three rings of the rigid arm. The terminal piperazine ring and the fluorescein moiety are unstructured, showing no clear electron density (Figure 2A). We identified two distinct inhibitor binding modes in our structure.

In the first binding mode, which was modeled with 20% occupancy, the bromobenzyl moiety is located within the arginine-patch formed by Arg534, Arg536, and Arg463. The Arg463 side-chain forms a π -cation interaction with the bromobenzyl group (3.5 Å) and simultaneously interacts with the nitrogen atom of the pyridine ring (3.2 Å; Figure 2A1). This conformation is identical to that of the previously observed binding mode of **3** (PDB code 4NGQ), but seems not to be the most favorable for **7**. This observation is supported by the fact that we detected electron density only for the first pyridine ring of the rigid arm, which suggests that the rigid arm is not very well-structured in this conformation.

In the second binding mode (Figure 2A2), the bromobenzyl group of **7** is not present within the arginine-patch and is located within the entrance funnel in two distinct conformations,

both modeled with 40% occupancy and differing only in the position of the bromobenzyl moiety. The rigid arm is positioned above the arginine-patch, with the pyridine ring forming a π -cation interaction with the side chain of Arg463 (3.6 Å). Arg463 is additionally stabilized by water-mediated hydrogen bonds between its guanidinium group (2.9 Å and 2.8 Å) and the carbonyl oxygen of **7** (2.6 Å). The stability of this conformation is also increased by a T-shaped stacking interaction of the piperazine ring and the Trp541 side chain (3.4 Å) and a π -cation interaction of the benzene ring and the Arg511 side chain (3.6 Å). These two residues form the so-called arene-binding site (ABS), which is involved in binding of the endogenous GCPII substrate folyl-poly- γ -L-glutamate.¹⁹ The high similarity of the binding modes of **7** and of the endogenous GCPII substrate folyl-di- γ -L-glutamate is illustrated in Figure 2B1 and B2.

The bromobenzyl group does not form any direct interactions with the protein in the second conformation, suggesting that its removal may lead to conformational stabilization and higher inhibitory potency. Interestingly, we investigated the inhibition potencies of the inhibitors with [K_i(**5**) = 49 pM] and without [K_i(**4**) = 71 pM] the bromobenzyl moiety and observed the opposite effect. This phenomenon could be explained by a potential second conformational state of **5**, with the bromobenzyl group bound within arginine-patch, which increases the overall entropy of the system.

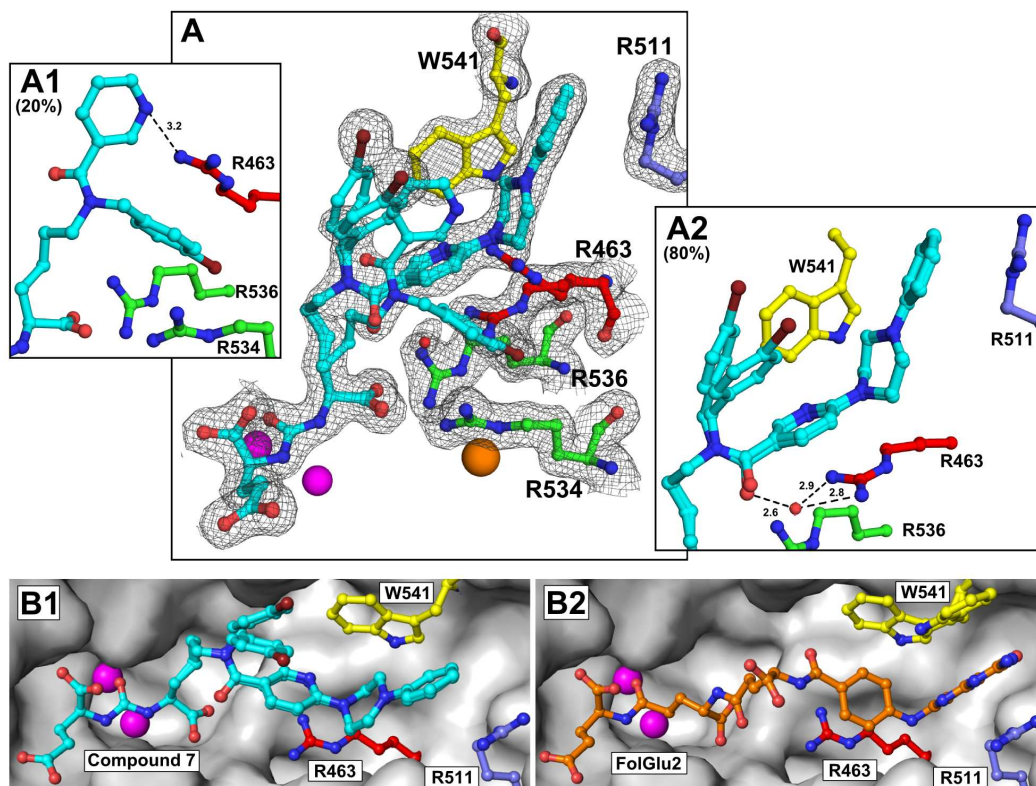


Figure 2. Binding modes of 7 in complex with Avi-GCPII (PDB code 4X3R). The inhibitor molecule and selected Avi-GCPII amino acid side chains are depicted in ball-and-stick representation with oxygen atoms colored red, nitrogen atoms blue, bromine atoms dark red, and carbon atoms color-coded. Zinc ions are shown as magenta spheres and the chloride ion as an orange sphere. **A:** Two different binding modes of 7 (depicted in cyan) are shown together with the $2F_o - F_o$ electron density map (contoured at 1σ). Amino acid side chains involved in binding of the inhibitor linker region are shown: R463 in red, R511 in blue, R534 and R536 in green, and W541 in yellow. The individual inhibitor binding modes are depicted in A1 and A2. The dashed lines (distances shown) indicate hydrogen bonds. The modeled occupancy of the given conformational state is shown. **B:** Comparison of the binding modes of 7 (B1) and folyl- γ -di-L-glutamate (FolGlu2; PDB code 4MCQ; B2). Color-coding is the same as in panel A with FolGlu2 depicted in orange. Selected parts of protein molecules are shown as gray surfaces.

Finally, to analyze the selectivity of our compounds, we tested their activity toward human GCPIII. As summarized in Figure 1, the overall inhibitory potency of all tested compounds is lower for GCPIII than GCPII, with the lead compound **1** showing 48-fold lower potency [$K_i(\mathbf{1}_{\text{GCPII}}) = 0.17 \text{ nM}$ vs. $K_i(\mathbf{1}_{\text{GCPIII}}) = 8.2 \text{ nM}$]. Further optimization of inhibitors that bind to GCPII exosites—the arginine-patch in the case of the bromobenzyl moiety (**2**) or ABS in the case of the rigid arm (**4**)—led to additional 7-fold and 29-fold increases in inhibitor selectivity, respectively. This mechanism seems to be additive because the combination of both motifs led to an approximately 100-fold increase in selectivity compared to parent compound, with the most selective compound (**6**) showing 6,600-fold greater potency toward GCPII than GCPIII [$K_i(\mathbf{6}_{\text{GCPII}}) = 110 \text{ pM}$ vs. $K_i(\mathbf{6}_{\text{GCPIII}}) = 730 \text{ nM}$]. The larger impact on inhibitor selectivity for the rigid arm moiety compared to the bromobenzyl moiety can be explained by different amino acids occupying the ABS (Trp541 for GCPII and Lys531 for GCPIII). Following this reasoning, any compound that utilizes the GCPII exosites for effective binding will likely show high selectivity for GCPII over GCPIII.

To demonstrate the general applicability and selectivity of these inhibitors, we created GCPII- and GCPIII-transfected cell lines using the inducible Tet-Off gene expression system, which enables regulation of the target protein expression by addition of doxycycline (dox). As shown in Figure 3A and B,

we were able to detect GCPII and GCPIII with monoclonal antibody²⁰ and also confirmed that both proteins were enzymatically active. Moreover, we were unable to detect GCPII or GCPIII expression and activity in the presence of dox, which demonstrated the high efficiency of our inducible expression system. For facile validation of our model system, we prepared direct fluorophore conjugates with inhibitors containing the rigid linker. We synthesized conjugates bearing either a fluorescein moiety (**7**) or DY-676 moiety (**S6**). Since **S6** displayed non-specific binding, we continued further experiments with **7**, which inhibited GCPII 1,900-fold more potently than GCPIII. Using both confocal microscopy and flow cytometry, we were able to selectively visualize GCPII but not GCPIII (Figure 3C and D).

Furthermore, we analyzed the selectivity of several common GCPII inhibitors described in the literature (2-PMPA,²¹ ZJ-43,²² DCIBzL²³) and one commercially available imaging agent (DKFZ-PSMA-11²⁴). The data summarized in Table 1 show that a simple inhibitor such as 2-PMPA, with just a P1' site-binding glutamate and zinc-binding group, is not highly selective. On the other hand, the urea-based inhibitor ZJ-43 (Glu-NH-C(O)-NH-Ile) already shows a significant increase in selectivity, which may be caused either by replacement of the zinc-binding group (phosphonate vs. urea) or by extension of the inhibitor to the P1 site.

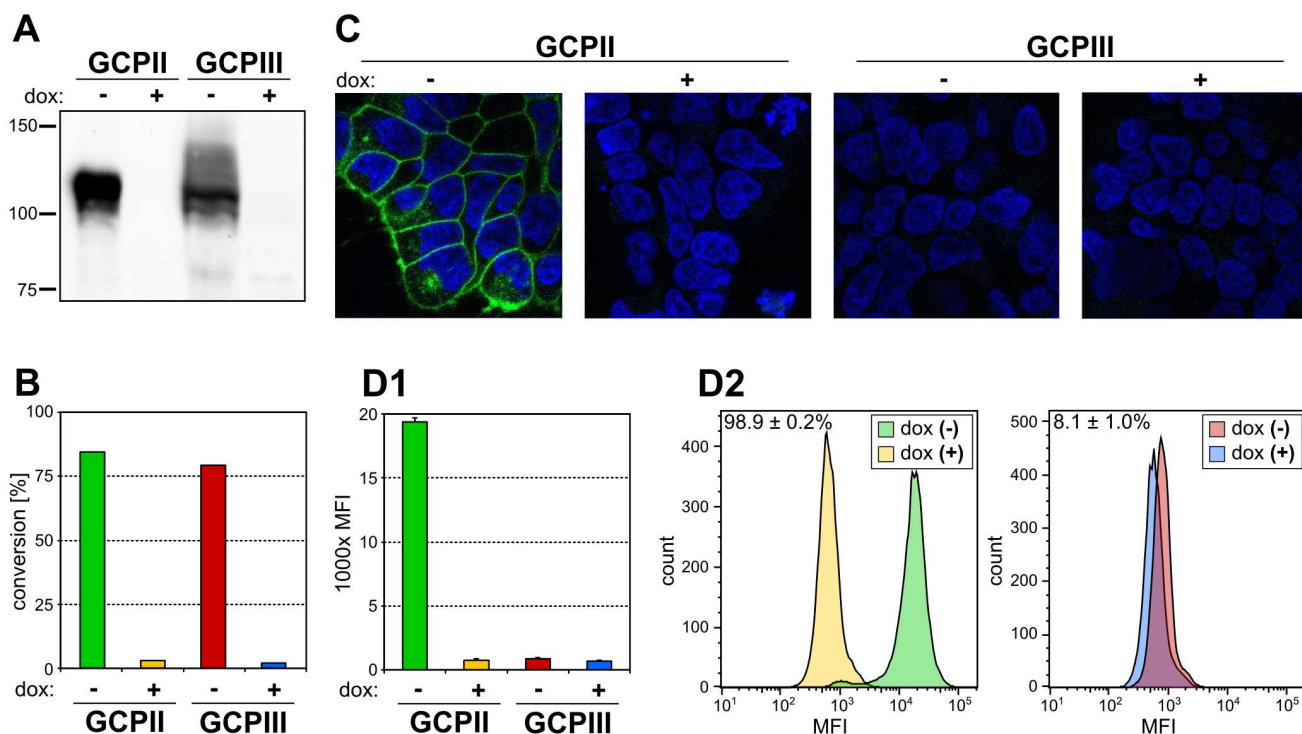


Figure 3. Analysis of the specific binding of 7 to GCPII and GCPIII-expressing cells. HEK293-Tet-Off cells stably transfected with pTRETightGCPII or pTRETightGCPIII were grown in the presence [dox(+)] or absence [dox(-)] of 200 nM doxycycline (dox). **A:** Western blot analysis of GCPII and GCPIII expression in HEK293 cells. Lysates were prepared from GCPII- and GCPIII-transfectants, loaded onto a gel (5 μ g and 100 μ g total protein, respectively), and analyzed by Western blot using GCP-04 monoclonal antibody, which recognizes both GCPII and GCPIII.²⁵ **B:** Enzymatic activity analysis of GCPII and GCPIII expression in HEK293 cells. The same cell lysate preparation used for Western blot analysis was probed for enzymatic activity toward NAAG, the endogenous substrate of both GCPII and GCPIII.¹¹ GCPII- and GCPIII-transfectant lysates (1 μ g total protein) were incubated for 15 h at 37 °C with 100 nM ³H-NAAG. Released ³H-L-glutamate was then separated from uncleaved ³H-NAAG on ion-exchange resin and detected using liquid scintigraphy. **C:** Confocal fluorescence microscopy of GCPII- and GCPIII-transfectants using 7. The cell transfectants were grown to approximately 20% confluence. Compound 7 (100 nM final concentration, green) was added into the growth media for 20 min, and the cell nuclei were subsequently stained with Hoechst dye (blue). All confocal images were taken using the same microscope settings and processed using ZEN 2011 software (Carl Zeiss Microscopy). **D:** Flow cytometry analysis of GCPII- and GCPIII-transfectants using 7. The cell transfectants were grown, harvested, and incubated in the presence of 100 nM 7 for 30 min. Then, the cells were analyzed by flow cytometry (fluorescence detection ex./em. 495 nm/519 nm). Each experiment was conducted in triplicate; 10,000 living cells were analyzed for each measurement. **D1:** Graph illustrating the mean fluorescence intensity (MFI) of analyzed transfectants. Data are shown as mean values with standard deviation (SD). **D2:** Histograms showing the population distribution based on MFI. Each histogram was created from a single representative experiment. GCPII-transfected cells expressing [dox(-)] and not expressing [dox(+)] GCPII are compared. The number in the top left corner indicates the percentage of the GCPII-expressing [dox(-)] population that has a higher MFI signal than the highest 5% of the population not expressing GCPII [dox(+)]. This number is shown as a mean of triplicate measurements with SD. A comparable histogram is shown for GCPIII-transfected cells.

Table 1. Inhibition constants of common GCPII inhibitors

	Avi-GCPII K_i [nM]	Avi-GCPIII K_i [nM]	selectivity
2-PMPA	0.28 ± 0.02	2.7 ± 0.1	10
ZJ-43	0.58 ± 0.03	150 ± 10	260
DKFZ-PSMA-11	0.018 ± 0.001	13 ± 1	720
DCIBzL	0.0030 ± 0.0001	2.5 ± 0.1	830

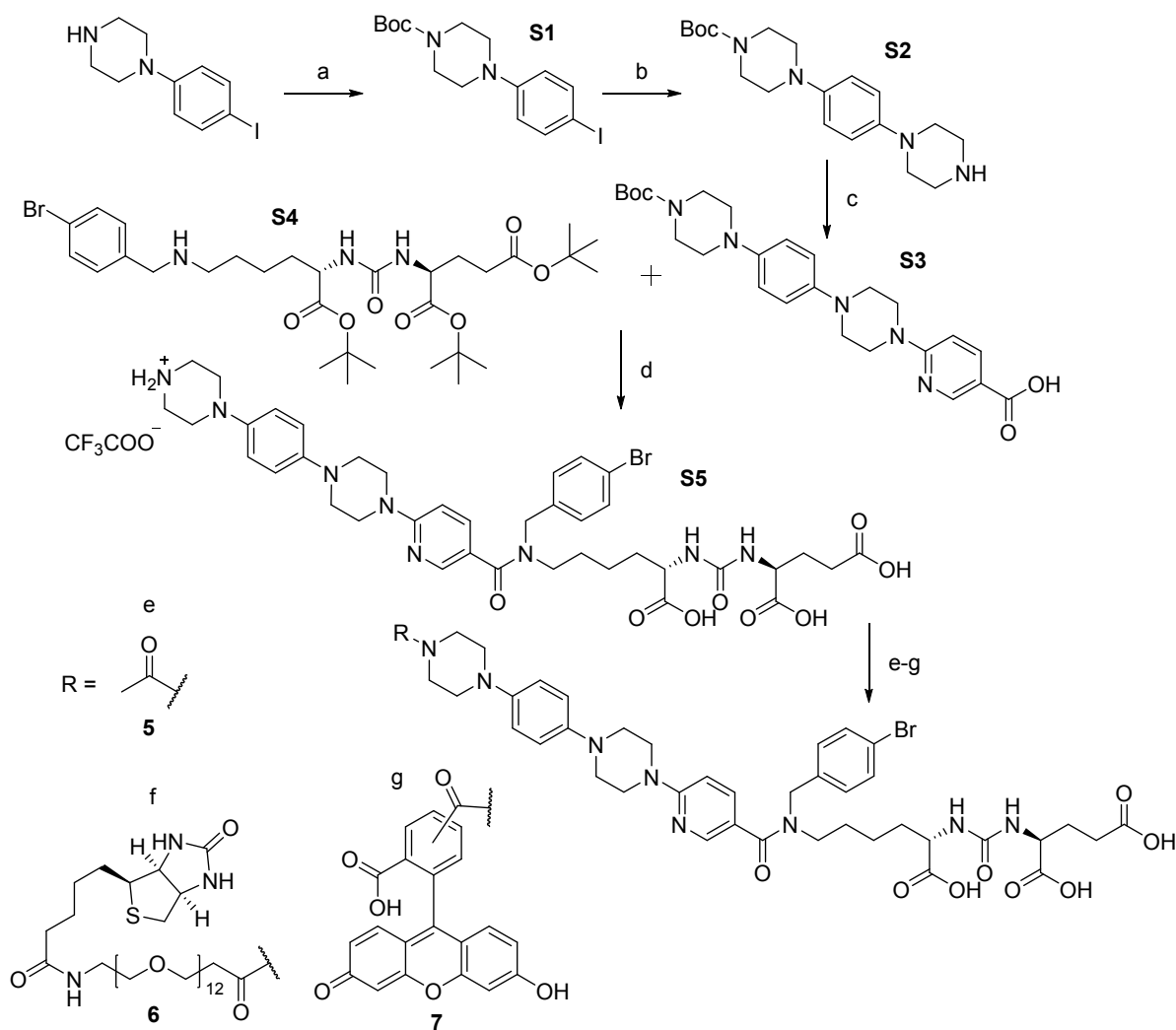
K_i values were determined as described in Figure 1 and are shown as mean values with SE from duplicate experiments.

Additional elongation of the inhibitor towards the S2 site of the enzyme (DKFZ-PSMA-11) led to further increase in the selectivity, suggesting that the entrance funnel of GCPII is more flexible than that of GCPIII and thus more prone to tol-

erate larger moieties. Therefore, it can be expected that any elongation of the GCPII inhibitor may lead to an increase in its selectivity. Nevertheless, the presented data, as well as data for DCIBzL, an inhibitor that binds to the GCPII arginine patch,²³ suggest that involvement of an exosite binding moiety further significantly increases the inhibitor's selectivity.

It should be noted that, despite its high selectivity, DKFZ-PSMA-11 is still able to inhibit GCPIII with a nanomolar inhibition constant ($K_i = 13$ nM) and thus may disrupt BCG metabolism. Generally, we believe that the determination of the selectivity of imaging agents (i.e., inhibitory activity towards GCPIII) is important for proper assessment of their working concentrations during imaging experiments to ensure that these imaging agents will exclusively target GCPII.

Scheme 1. Synthesis of compounds 5, 6, and 7.



36 a) Boc_2O , Et_3N , DCM; b) piperazine, Pd_2dba_3 , Xantphos, $\text{KO}^t\text{-Bu}$, Tol, 80°C ; c) 6-chloronicotinic acid, DIEA, DMAc, 130°C ; d) 1) TBTU, DIEA, DMF, 2) TFA; e) Ac-NHS, DIEA, DMF; f) Biotin-PEG₁₂-NHS, DIEA, DMF; g) 5(6)-carboxyfluorescein TBTU, DIEA, DMF

CONCLUSION

37
38
39
40
41
42 In this work, we developed potent and highly specific inhibitors of GCPII by structure-aided drug design. The specificity was achieved by exploiting exosites identified in the structure of GCPII that are not present in the structure of its closest homolog, human GCPIII. We designed a structurally rigid linker that not only ensures high selectivity but also enables efficient connection of a GCPII inhibitor with other functional moieties, such as a fluorophore (7) or biotin (6). Finally, using GCPII and GCPIII-transfected mammalian cells, we demonstrated high efficiency of 7 as a laboratory tool for facile and specific GCPII visualization.

EXPERIMENTAL SECTION

43
44
45
46
47
48
49
50
51
52
53
54
55
56
57
58
59
60
Organic synthesis. All chemicals were purchased from Sigma-Aldrich, unless stated otherwise. All inhibitors tested in biological assays were purified on a preparative scale Waters Delta 600 HPLC instrument (flow rate 7 mL/min, gradient

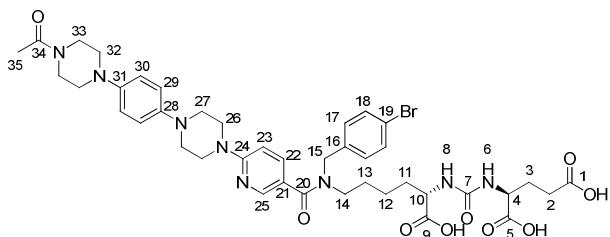
shown for each compound, including R_t), equipped with a Waters SunFire C18 OBD Prep Column, 5 μm , 19 x 150 mm.

The purity of compounds was tested on an analytical Jasco PU-1580 HPLC (flow rate 1 mL/min, invariable gradient 2-100% ACN in 30 min, R_t shown for each compound) equipped with a Watrex C18 Analytical Column, 5 μm , 250 x 5 mm. The final inhibitors were all of at least 99% purity. Structure was further confirmed by HRMS using an LTQ Orbitrap XL (Thermo Fisher Scientific) and by NMR (Bruker Avance™ 500 MHz equipped with a cryoprobe or Bruker Avance™ 400 MHz).

The synthesis and characterization of 1, 2, and 3 have been previously described.¹⁸

Compounds 5, 6, and 7 were synthesized as shown in Scheme 1.

ZJ-43 was prepared as previously described,²² 2-PMPA was a kind gift from Barbara S. Slusher, DCIBzL was a kind gift from Cyril Barinka, and DKFZ-PSMA-11 was purchased from ABX Advanced Biochemical Compounds.



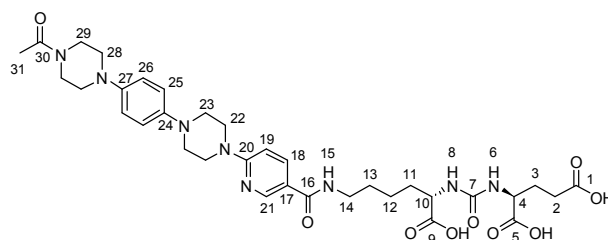
Compound 5: *(S)*-2-(3-((*S*)-5-(6-(4-(4-(4-acetylpiperazin-1-yl)phenyl)piperazin-1-yl)-N-(4-bromobenzyl)nicotinamido)-1-carboxypentyl)ureido)pentanedioic acid. **S5** (35 mg, 37 μmol , 1.0 eq) was dissolved in 0.5 mL DMF along with 20 μL DIEA (114 μmol , 3.0 eq). To this mixture, 11.5 mg of 2,5-dioxopyrrolidin-1-yl acetate (73 μmol , 2.0 eq) was added in one portion, and the reaction was stirred overnight. After 16 h, volatiles were evaporated, and the crude product was purified by preparative scale HPLC (grad: 15-50% ACN in 60 min, R_t = 35 min). **$^1\text{H NMR}$** (500 MHz, DMSO): δ 8.22 (bs, 1H, H-25), 7.67 (d, J = 6.9 Hz, 1H, H-22), 7.55 (d, J = 8.4 Hz, 2H, H-18), 7.18 (m, 6H, H-17, H-29, H-30), 6.98 (d, J = 8.8 Hz, 1H, H-23), 6.33 (d, J = 8.1 Hz, 1H, H-6), 6.30 (d, J = 8.1 Hz, 1H, H-8), 4.58 (s, 2H, H-15), 4.10 (dd, J = 13.1, 7.8 Hz, 1H, H-4), 4.04 (bm, 1H, H-10), 3.81 (bs, 4H, H-26), 3.64 (bs, 4H, H-33), 3.37 (bs, 4H, H-27), 3.20 (bm, 6H, H-32, H-14, partial overlap with residual peak from water), 2.31 – 2.16 (m, 2H, H-2), 2.05 (s, 3H, H-35), 1.92 (ddt, J = 12.0, 9.1, 6.0 Hz, 1H, H-3a), 1.71 (ddt, J = 12.0, 9.1, 6.8 Hz, 1H, H-3b), 1.65 – 1.38 (m, 4H, H-11, H-13), 1.20 (d, J = 27.7 Hz, 2H, H-12). **$^{13}\text{C NMR}$** (126 MHz, DMSO): δ 174.48 (C-9), 174.19 (C-5), 173.76 (C-1), 169.01 (C-20), 168.38 (C-34), 158.35 (q, TFA), 157.91 (C-24), 157.26 (C-7), 150.61 (C-25), 145.58 (C-31, C-28), 137.19 (C-18, C-22), 131.48 (C-17), 121.16 (C-19), 120.22 (C-29), 118.27 (C-30), 117.39 (C-21), 115.51 (q, J = 290.8 Hz, TFA), 106.77 (C-23), 52.12 (C-4), 51.65 (C-10), 50.80 (C-32), 44.82-43.62 (C-14, C-15, C-26, C-27, C-33), 31.71 (C-11), 29.90 (C-2), 27.54 (C-13), 27.02 (C-3), 22.36 (C-12), 21.19 (C-35). **Analytical HPLC** R_t = 17.4 min. **HRMS** (ESI+) m/z for $\text{C}_{41}\text{H}_{50}\text{O}_9\text{N}_8\text{Br}$ [$\text{M}+\text{H}$]⁺ calc. 877.28896, found 877.28658.

Compound 6: *(S)*-2-(3-((*S*)-5-(N-(4-bromobenzyl)-6-(4-(4-(4-(41-oxo-45-(3a*S*,4*S*,6a*R*)-2-oxohexahydro-1*H*-thieno[3,4-*d*]imidazol-4-yl)-4,7,10,13,16,19,22,25,28,31,34,37-dodecaoxa-40-azapentatetracontan-1-yl)piperazin-1-yl)phenyl)piperazin-1-yl)nicotinamido)-1-carboxypentyl)ureido)pentanedioic acid. **S5** (18 mg, 21 μmol , 1.1 eq) was dissolved in 0.5 mL DMF along with DIEA (8 μL , 48 μmol , 2.5 eq). To this mixture, biotin-PEG₁₂-COONHS (18 mg, 19 μmol , 1.0 eq) was added in one portion, and the reaction was left to proceed overnight. After 12 h, volatiles were evaporated, and the product was purified by preparative scale HPLC (grad: 30-80% ACN in 50 min, R_t = 22 min). Pure product (8 mg) was isolated upon dry freezing (isolated yield = 25%). **Analytical HPLC** R_t = 18.3 min. **HRMS** (ESI-) m/z for $\text{C}_{76}\text{H}_{115}\text{O}_{23}\text{N}_{11}\text{BrS}$ [$\text{M}-\text{H}$]⁻ calc. 1660.70768, found 1660.70441.

Compound 7: *(S)*-2-(3-((*S*)-5-(N-(4-bromobenzyl)-6-(4-(4-(4-(4-carboxy-3-(6-hydroxy-3-oxo-3*H*-xanthen-9-yl)benzoyl)piperazin-1-yl)phenyl)piperazin-1-yl)nicotinamido)-1-carboxypentyl)ureido)pentanedioic acid. A mixture of 5- and 6-carboxy fluorescein (12 mg, 31 μmol , 1.0 eq) and DIEA (19 μL , 110 μmol , 3.5 eq) were dissolved in 0.5 mL DMF, and TBTU (10 mg, 31 μmol , 1.0 eq) was added in one portion. The reaction mixture was stirred for 30 min to

activate the carboxylic acid. Then, **S5** (30 mg, 31 μmol , 1.0 eq) dissolved in 0.5 mL DMF was added to the mixture. The reaction was left to proceed overnight. Volatiles were then evaporated, and the crude product was purified by preparative scale HPLC (grad: 15-50% ACN in 50 min, R_t = 43 min). 12 Pure product (12 mg) was isolated upon dry freezing (isolated yield = 32%). **Analytical HPLC** R_t = 19.1 min. **HRMS** (ESI-) m/z for $\text{C}_{60}\text{H}_{58}\text{O}_{14}\text{N}_8\text{Br}$ [$\text{M}-\text{H}$]⁻ calc. 1193.32613, found 1193.32656.

Synthesis and characterization of 4.



Compound 4: *(S)*-2-(3-((*S*)-5-(6-(4-(4-(4-acetylpiperazin-1-yl)phenyl)piperazin-1-yl)nicotinamido)-1-carboxypentyl)ureido)pentanedioic acid. The synthesis of **4** was nearly identical to that of the bromobenzylated derivative **5** with the difference that a derivative without amine substitution was used in step d. The final product precipitated from a mixture of ACN/ H_2O (2:1). The isolated yield after the 3 steps was 15%. **$^1\text{H NMR}$** (500 MHz, DMSO) δ 8.60 (d, J = 2.7 Hz, 1H, H-21), 8.25 (t, J = 5.6 Hz, 1H, H-15), 7.96 (dd, J = 9.0, 2.5 Hz, 1H, H-18), 6.95 – 6.87 (m, 5H, H-25, H-26, H-19), 6.33 (d, J = 8.3 Hz, 1H, H-6), 6.31 (d, J = 8.3 Hz, 1H, H-8), 4.12 – 4.02 (m, 2H, H-4, H-10), 3.74 – 3.70 (m, 4H, H-22), 3.55 (dd, J = 10.4, 5.8 Hz, 4H, H-23), 3.21 (dd, J = 13.1, 6.7 Hz, 2H, H-14), 3.12 – 3.07 (m, 4H, H-29), 3.03 – 2.92 (m, 4H, H-28), 2.31 – 2.17 (m, 2H, H-2), 2.03 (s, 3H, H-31), 1.95 – 1.87 (m, 1H, H-3a), 1.75 – 1.63 (m, 1H, H-3b), 1.60 – 1.44 (m, 3H, H-11a, H-13), 1.37 – 1.20 (m, 3H, H-11b, H-12). **$^{13}\text{C NMR}$** (126 MHz, DMSO) δ 174.58 (C-9), 174.22 (C-5), 173.76 (C-1), 168.21 (C-16), 164.79 (C-30), 159.71 (C-20), 157.30 (C-7), 147.79 (C-21), 144.98 (C-24 or C-27), 144.79 (C-24 or C-27), 136.50 (C-18), 118.92 (C-26), 117.53 (C-25), 117.36 (C-17), 105.67 (C-19), 52.29 (C-4), 51.65 (C-10), 50.01 (C-28), 49.61, 49.38, 45.66, 44.38, 40.82 (C-14, C-15, C-26, C-27, C-33), 31.83 (C-11), 29.93 (C-2), 28.98 (C-13), 27.54 (C-3), 22.71 (C-12), 21.24 (C-31). **Analytical HPLC** R_t = 14.0 min. **HRMS** (ESI-) m/z for $\text{C}_{34}\text{H}_{45}\text{O}_9\text{N}_8$ [$\text{M}-\text{H}$]⁻ calc. 709.33040, found 709.33016.

Description and characterization of the reaction intermediates (**S1-S6**) and descriptions of all biochemical and molecular biology methods used are provided in the Supporting Information.

ASSOCIATED CONTENT

Supporting Information. Descriptions of the synthesis and characterization of intermediate compounds, descriptions of biochemical and molecular biology techniques used in this study, and a table with crystallographic data collection and refinement statistics are shown. This material is available free of charge via the Internet at <http://pubs.acs.org>.

AUTHOR INFORMATION

Corresponding Authors

* JK; Institute of Organic Chemistry and Biochemistry, ASCR, v.v.i.; Flemingovo n. 2, Prague 6, 166 10, Czech Republic; tel: 00420 220 183 218, fax: 00420 220 183 578;

Email: konval@uochb.cas.cz

* PS; Institute of Organic Chemistry and Biochemistry, ASCR, v.v.i.; Flemingovo n. 2, Prague 6, 166 10, Czech Republic; tel: 00420 220 183 452, fax: 00420 220 183 578;

Email: pavelsacha@gmail.com

Author Contributions

All authors have given approval to the final version of the manuscript.

‡These authors contributed equally.

Funding Sources

This work was supported by grant P208-12-G016 (Center of Excellence) from the Grant Agency of the Czech Republic and NPU I project LO 1302 from the Ministry of Education of the Czech Republic.

ACKNOWLEDGMENT

We would like to acknowledge Sebastian Zoll, Ph.D., for collecting the x-ray dataset on synchrotron and Petr Pachel, Ph.D., for integration and scaling of this dataset.

ABBREVIATIONS

ABS, arene-binding site; Avi-GCPII/III, extracellular portions of GCPII (44-750) or GCPIII (36-740) with N-terminal AviTEV tag; dox, doxycycline; GCPII/III, glutamate carboxypeptidase II/III; NAAG, N-acetyl-L-aspartyl-L-glutamate; PCa, prostate carcinoma; MFI, mean fluorescence intensity; PSMA, prostate-specific membrane antigen

REFERENCES

- (1) Siegel, R.; Ma, J.; Zou, Z.; Jemal, A. Cancer statistics, 2014. *CA Cancer J Clin* **2014**, *64*, 9-29.
- (2) Foss, C. A.; Mease, R. C.; Cho, S. Y.; Kim, H. J.; Pomper, M. G. GCPII Imaging and Cancer. *Current Medicinal Chemistry* **2012**, *19*, 1346-1359.
- (3) Ghosh, A.; Heston, W. D. W. Tumor target prostate specific membrane antigen (PSMA) and its regulation in prostate cancer. *Journal of Cellular Biochemistry* **2004**, *91*, 528-539.
- (4) Huber, F.; Montani, M.; Sulser, T.; Jaggi, R.; Wild, P.; Moch, H.; Gevensleben, H.; Schmid, M.; Wyder, S.; Kristiansen, G. Comprehensive validation of published immunohistochemical prognostic biomarkers of prostate cancer-what has gone wrong? A blueprint for the way forward in biomarker studies. *Br J Cancer* **2014**.
- (5) Tagawa, S. T.; Akhtar, N. H.; Nikolopoulou, A.; Kaur, G.; Robinson, B.; Kahn, R.; Vallabhajosula, S.; Goldsmith, S. J.; Nanus, D. M.; Bander, N. H. Bone marrow recovery and subsequent chemotherapy following radiolabeled anti-prostate-specific membrane antigen monoclonal antibody j591 in men with metastatic castration-resistant prostate cancer. *Front Oncol* **2013**, *3*, 214.
- (6) Haffner, M. C.; Kronberger, I. E.; Ross, J. S.; Sheehan, C. E.; Zitt, M.; Muhlmann, G.; Ofner, D.; Zelger, B.; Ensinger, C.; Yang, X. M. J.; Geley, S.; Margreiter, R.; Bander, N. H. Prostate-specific membrane antigen expression in the neovasculature of gastric and colorectal cancers. *Human Pathology* **2009**, *40*, 1754-1761.
- (7) Chang, S. S.; Reuter, V. E.; Heston, W. D.; Bander, N. H.; Grauer, L. S.; Gaudin, P. B. Five different anti-prostate-specific membrane antigen (PSMA) antibodies confirm PSMA expression in tumor-associated neovasculature. *Cancer Res* **1999**, *59*, 3192-3198.
- (8) Chen, Y.; Pullambhatla, M.; Banerjee, S. R.; Byun, Y.; Stathis, M.; Rojas, C.; Slusher, B. S.; Mease, R. C.; Pomper, M. G. Synthesis and biological evaluation of low molecular weight fluorescent imaging agents for the prostate-specific membrane antigen. *Bioconjug Chem* **2012**, *23*, 2377-2385.
- (9) Kovar, J. L.; Cheung, L. L.; Simpson, M. A.; Olive, D. M. Pharmacokinetic and Biodistribution Assessment of a Near Infrared-

Labeled PSMA-Specific Small Molecule in Tumor-Bearing Mice. *Prostate Cancer* **2014**, *2014*, 104248.

(10) Mease, R. C.; Foss, C. A.; Pomper, M. G. PET imaging in prostate cancer: focus on prostate-specific membrane antigen. *Curr Top Med Chem* **2013**, *13*, 951-962.

(11) Hlouchova, K.; Barinka, C.; Klusak, V.; Sacha, P.; Mlcochova, P.; Majer, P.; Rulisek, L.; Konvalinka, J. Biochemical characterization of human glutamate carboxypeptidase III. *J Neurochem* **2007**, *101*, 682-696.

(12) Pangalos, M. N.; Neefs, J. M.; Somers, M.; Verhasselt, P.; Bekkers, M.; van der Helm, L.; Fraiponts, E.; Ashton, D.; Gordon, R. D. Isolation and expression of novel human glutamate carboxypeptidases with N-acetylated alpha-linked acidic dipeptidase and dipeptidyl peptidase IV activity. *J Biol Chem* **1999**, *274*, 8470-8483.

(13) Collard, F.; Vertommen, D.; Constantinescu, S.; Buts, L.; Van Schaffingen, E. Molecular identification of beta-citrylglutamate hydrolase as glutamate carboxypeptidase 3. *J Biol Chem* **2011**, *286*, 38220-38230.

(14) Miyake, M.; Kume, S.; Kakimoto, Y. Correlation of the level of beta-citryl-L-glutamic acid with spermatogenesis in rat testes. *Biochim Biophys Acta* **1982**, *719*, 495-500.

(15) Narahara, M.; Tachibana, K.; Adachi, S.; Iwasa, A.; Yukii, A.; Hamada-Kanazawa, M.; Kawai, Y.; Miyake, M. Immunocytochemical localization of beta-citryl-L-glutamate in primary neuronal cells and in the differentiation of P19 mouse embryonal carcinoma cells into neuronal cells. *Biol Pharm Bull* **2000**, *23*, 1287-1292.

(16) Hamada-Kanazawa, M.; Kouda, M.; Odani, A.; Matsuyama, K.; Kanazawa, K.; Hasegawa, T.; Narahara, M.; Miyake, M. beta-Citryl-L-glutamate is an endogenous iron chelator that occurs naturally in the developing brain. *Biol Pharm Bull* **2010**, *33*, 729-737.

(17) Hamada-Kanazawa, M.; Narahara, M.; Takano, M.; Min, K. S.; Tanaka, K.; Miyake, M. beta-Citryl-L-glutamate acts as an iron carrier to activate aconitase activity. *Biol Pharm Bull* **2011**, *34*, 1455-1464.

(18) Tykvar, J.; Schimer, J.; Barinkova, J.; Pachel, P.; Postova-Slavetinska, L.; Majer, P.; Konvalinka, J.; Sacha, P. Rational design of urea-based glutamate carboxypeptidase II (GCPII) inhibitors as versatile tools for specific drug targeting and delivery. *Bioorg Med Chem* **2014**, *22*, 4099-4108.

(19) Navratil, M.; Ptacek, J.; Sacha, P.; Starkova, J.; Lubkowski, J.; Barinka, C.; Konvalinka, J. Structural and biochemical characterization of the folyl-poly-gamma-l-glutamate hydrolyzing activity of human glutamate carboxypeptidase II. *FEBS J* **2014**, *281*, 3228-3242.

(20) Sacha, P.; Zamecnik, J.; Barinka, C.; Hlouchova, K.; Vicha, A.; Mlcochova, P.; Hilgert, I.; Eckschlager, T.; Konvalinka, J. Expression of glutamate carboxypeptidase II in human brain. *Neuroscience* **2007**, *144*, 1361-1372.

(21) Jackson, P. F.; Cole, D. C.; Slusher, B. S.; Stetz, S. L.; Ross, L. E.; Donzanti, B. A.; Trainor, D. A. Design, synthesis, and biological activity of a potent inhibitor of the neuropeptidase N-acetylated alpha-linked acidic dipeptidase. *J Med Chem* **1996**, *39*, 619-622.

(22) Olszewski, R. T.; Bukhari, N.; Zhou, J.; Kozikowski, A. P.; Wroblewski, J. T.; Shamimi-Noori, S.; Wroblewska, B.; Bzdega, T.; Vicini, S.; Barton, F. B.; Neale, J. H. NAAG peptidase inhibition reduces locomotor activity and some stereotypes in the PCP model of schizophrenia via group II mGluR. *J Neurochem* **2004**, *89*, 876-885.

(23) Wang, H.; Byun, Y.; Barinka, C.; Pullambhatla, M.; Bhang, H. E.; Fox, J. J.; Lubkowski, J.; Mease, R. C.; Pomper, M. G. Biososterism of urea-based GCPII inhibitors: Synthesis and structure-activity relationship studies. *Bioorg Med Chem Lett* **2010**, *20*, 392-397.

(24) Eder, M.; Schafer, M.; Bauder-Wust, U.; Hull, W. E.; Wangler, C.; Mier, W.; Haberkorn, U.; Eisenhut, M. ⁶⁸Ga-complex lipophilicity and the targeting property of a urea-based PSMA inhibitor for PET imaging. *Bioconjug Chem* **2012**, *23*, 688-697.

(25) Tykvar, J.; Navratil, V.; Sedlak, F.; Corey, E.; Colombatti, M.; Fracasso, G.; Koukolik, F.; Barinka, C.; Sacha, P.; Konvalinka, J. Comparative analysis of monoclonal antibodies against prostate-specific membrane antigen (PSMA). *Prostate* **2014**, *74*, 1674-1690.

Insert Table of Contents artwork here

